JOURNAL OF THE ROYAL SOCIETY Interface

rsif.royalsocietypublishing.org

Research

Cite this article: Klumpers DD, Mao AS, Smit TH, Mooney DJ. 2014 Linear patterning of mesenchymal condensations is modulated by geometric constraints. *J. R. Soc. Interface* **11**: 20140215.
http://dx.doi.org/10.1098/rsif.2014.0215

Received: 28 February 2014
Accepted: 6 March 2014

Subject Areas:
bioengineering

Keywords:
pattern formation, vertebral column, mesenchymal condensation, morphogenesis, geometry, skeletal development

Author for correspondence:
David J. Mooney
e-mail: mooneyd@seas.harvard.edu

Electronic supplementary material is available at http://dx.doi.org/10.1098/rsif.2014.0215 or via http://rsif.royalsocietypublishing.org.

Royal Society Publishing

Linear patterning of mesenchymal condensations is modulated by geometric constraints

Darinka D. Klumpers[1,2,3], Angelo S. Mao[1,2], Theo H. Smit[3] and David J. Mooney[1,2]

[1]School of Engineering and Applied Sciences, Harvard University, 29 Oxford St., Cambridge, MA 02138, USA
[2]Wyss Institute for Biologically Inspired Engineering, Harvard University, 3 Blackfan Circle, Boston, MA 02115, USA.
[3]Department of Orthopedic Surgery, Research Institute MOVE, VU University Medical Center, De Boelelaan 1117, 1081 HV Amsterdam, The Netherlands

The development of the vertebral column starts with the formation of a linear array of mesenchymal condensations, forming the blueprint for the eventual alternating pattern of bone and cartilage. Despite growing insight into the molecular mechanisms of morphogenesis, the impact of the physical aspects of the environment is not well understood. We hypothesized that geometric boundary conditions may play a pivotal role in the linear patterning of condensations, as neighbouring tissues provide physical constraints to the cell population. To study the process of condensation and the patterning thereof under tightly controlled geometric constraints, we developed a novel *in vitro* model that combines micropatterning with the established micromass assay. The spacing and alignment of condensations changed with the width of the cell adhesive patterns, a phenomenon that could not be explained by cell availability alone. Moreover, the extent of chondrogenic commitment was increased on substrates with tighter geometric constraints. When the *in vivo* pattern of condensations was investigated in the developing vertebral column of chicken embryos, the measurements closely fit into the quantitative relation between geometric constraints and inter-condensation distance found *in vitro*. Together, these findings suggest a potential role of geometric constraints in skeletal patterning in a cellular process of self-organization.

1. Introduction

During the growth and development of the embryo, patterning events give rise to structurally and functionally complex tissues. These morphogenetic events involve an intricate interplay of cellular processes and result in robust outcomes. The role of molecular signalling pathways in achieving these complex outcomes has been studied extensively, however, the impact of physical cues is just starting to be unravelled [1–5]. For example, it was shown recently that the looping pattern of the gut is driven by the forces that arise from differential growth [6], while the pattern of villi lining the gut wall is determined by buckling and folding of the tissue owing to growth under spatial restrictions [7]. Investigations into the role of physical cues in embryogenesis are gaining momentum owing to innovative techniques that allow characterization, modelling and perturbation of developmental processes [1,8–10]. However, the potential role of physical cues in the development of many complex tissue patterns is still to be discovered.

One of the most fundamental and conserved patterns of the vertebrate body plan is the vertebral column. With its alternating pattern of bony elements and cartilaginous hinges, it provides form and stability as well as flexibility to the vertebrate body. Both the bone and cartilage tissue of the vertebral column originate from sclerotomal cells, a mesenchymal cell population originating from the ventral–medial region of the somites [11]. After dissociation from the residual epithelial component of the somites, the sclerotomal cells accumulate around the notochord and subsequently form a robust linear array of mesenchymal

condensations [11,12]. Mesenchymal condensation is the first stage in bone development [13–16] and an essential step in skeletal patterning since the position, size and number of skeletal elements is established at this stage [17,18].

Mesenchymal condensation primarily involves an increase in local cell density [16,19], which appears to be mainly mediated through local cell movements rather than locally altered proliferation rates [20,21]. It is thought that these local cell rearrangements are predominantly mediated by passive ECM-driven movements and dragging and pushing by neighbouring cells, rather than active cell migration [22–24]. The dominant matrix components in this developmental stage are hyaluronic acid and fibronectin (FN) [25–29]. An increase in specific cell–cell contacts associated with mesenchymal condensation, mediated through N-cadherin and NCAM, facilitates cell–cell communication and is presumably involved in triggering the onset of chondrogenic differentiation [30–32]. This model is in line with the general notion that a high cell density is required for chondrogenesis [33,34].

The fundamental importance of mesenchymal condensation in skeletal development has motivated the development of *in vitro* models that recapitulate the early stages of skeletogenesis [35,36]. One *in vitro* model that is often used to study mesenchymal condensation is the micromass assay [37,38]. Typically, pre-chondrogenic cells are isolated from embryonic mouse or chicken limb buds and plated in a high-density drop. Within this high-density culture, condensations spontaneously appear within several days, followed by chondrogenic commitment and concomitant deposition of specific matrix components. Only embryonic cells seem to go through this specific process, as studies using adult or immortalized mesenchymal cells show different results [39,40]. The micromass model has been used to unravel cellular and molecular events involved in condensation as well as to investigate the role of a variety of signalling molecules in skeletal development [13,41,42]. However, physical cues such as the spatial restrictions set by neighbouring tissues are not taken into account in this model.

Micropatterning techniques, whereby cell adhesive islands are created in order to restrict single or multicellular cultures to specific geometries, have facilitated the study of the effect of geometric boundary conditions on a range of cellular events [43]. It has been shown that single-cell shape can control the switch between cell cycle advancement and apoptosis in certain cell types [44], while controlling the geometry of multicellular cultures elucidated emergent patterns of proliferation as well as differentiation [45–47]. Micropatterning, when combined with the micromass culture, could provide a useful tool to test the role of geometric boundary conditions in the supracellular process of condensation and skeletal patterning.

This study addresses the hypothesis that geometric constraints provided to mesenchymal cells determine their condensation pattern. This hypothesis was investigated by combining an *in vitro* cell patterning technique with the established micromass assay. Freshly isolated mesenchymal cells from chicken embryonic limb buds were used, as this has been proven to be an appropriate cell model for pre-chondrogenic condensation [13,37,38]. We demonstrate that geometric constraints affect linear patterning of condensations as well as subsequent chondrogenic differentiation. Moreover, measurements of the pattern of condensations in the developing vertebral column in the chicken embryo closely fit into the quantitative relation between geometric constraints and inter-condensation distance established by this new *in vitro* model.

2. Material and methods

2.1. Cell isolation and culture

Pre-chondrogenic limb bud cells were freshly isolated from chicken embryos for each experiment. Chicken eggs (White Leghorn, premium specific pathogen-free) were purchased from Charles River Laboratories (New York, NY, USA) and set to incubate at 37°C and 60% humidity. After 3 days of incubation, the embryos were staged and returned to the incubator. At Hamburger Hamilton stage 21–23 [48], the wing buds were dissected in PBS using a Leica stereomicroscope. Dissected limb buds were incubated in 0.5% trypsin for 12 min at room temperature and transferred to 10% ice-cold chicken serum in PBS. The ectoderm layer was subsequently manually removed from the limb buds. Buds were then suspended in DMEM-F12 culture medium containing 10% FBS and 1% penicillin and streptomycin (referred to as complete medium) and pipetted up and down to create a single-cell suspension. After straining through a 40 µm filter to remove cell clumps, the cells were counted, centrifuged and resuspended in complete medium to obtain a concentration of 6×10^6 cells ml^{-1}. A drop of 60 µl cell suspension was then spread onto the patterned area (approx. 75 mm^2) that was obtained as described in the following section (figure 1*a*(iv)). The cell seeding density was optimized during preliminary experiments which showed that lower cell densities lead to compromised cell survival, while higher cell densities mainly resulted in a larger fraction of cells not attaching to the substrate (data not shown). The plates were incubated at 37°C and 5% CO_2 for 1 h to allow the cells to attach to their substrate. Subsequently, the cultures were washed once to remove unattached cells and then 2.5 ml of DMEM-F12 containing 2% FBS and 1% penicillin and streptomycin was added per well. For specific experiments, the culture medium was supplemented with rhTGF-β3, rhBMP2 or rmFGF8 (R&D systems) at the indicated concentrations. The culture medium was refreshed after 24 h and cultures were terminated after 2.5 days.

2.2. Microchannel patterning

Polydimethylsiloxane (PDMS) moulds for creating cell adhesive islands were fabricated by soft lithography. Negative photo resist SU-8 2100 (MicroChem, Newton, MA, USA) was deposited onto clean silicon wafers to a thickness of 130 µm and patterned by exposure to UV light through a transparency photomask (CAD/Art Services, Bandon, OR, USA). PDMS moulds were made by mixing PDMS base and curing agent (Sylgard 184 silicone elastomer kit) in a 10 : 1 ratio and pouring onto the patterned silicon wafer. The PDMS was cured overnight at 65°C after which individual moulds were cut out. Each mould contained raised features 300 µm wide and 8 mm long (figure 1*b*). The width between raised features was 100, 150, 200, 250 or 300 µm. The moulds were stored in 70% ethanol until use. To create FN islands, the moulds were first sonicated in a water bath for 60 min. They were then dipped in dH_2O and placed in a 65°C oven to dry for 30 min. The PDMS moulds were subsequently subjected to O_2 plasma treatment for 5 min. Simultaneously, a non-tissue culture six-well plate was UV treated for 7 min. Each mould was then placed features-down in the centre of a well in the six-well plate, creating microchannels. A 50 µl drop of 25 µg ml^{-1} FN (bovine, Sigma) in dH_2O was placed directly next to the moulds and the solution was immediately drawn into the microchannels by capillary forces (figure 1*a*(i)). To create the non-patterned substrate, a 50 µl drop of FN solution was placed in the centre of the well in the absence of a PDMS mould. The drop was spread to cover the same surface area as the patterned substrates, leading to a similar adhesion ligand density. The FN solution was incubated at room temperature for 1 h. The solution was then carefully aspirated and the plates were

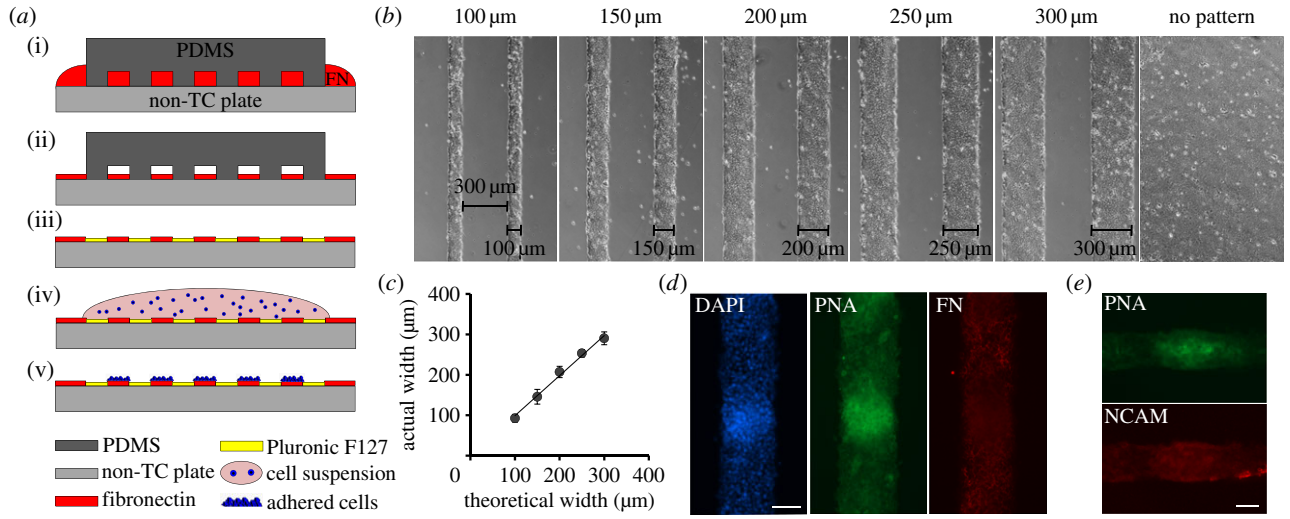

Figure 1. Experimental model. (*a*) Schematic of cell patterning procedure; (i) PDMS moulds are placed onto a non-tissue culture-treated plate, and an FN solution fills the channels of the mould. (ii) After 1 h of incubation, the FN solution is aspirated. (iii) After drying, the PDMS mould is removed and the plate is treated with Pluronic, which coats the non-patterned surface and leaves it non-adherent. (iv) A drop of cell suspension is spread over the patterned area. (v) The cells adhere to the FN patterns only. (*b*) Phase contrast micrographs of pre-chondrogenic cells cultured on linear adhesive islands or non-patterned substrates taken after 24 h in culture. The island width varies from 100 to 300 µm, while the non-adhesive space between islands is 300 µm wide for all conditions. (*c*) Plot indicating the correlation between the theoretical island width and the actual island width measured during cell culture. (*d*) Fluorescent micrographs of pre-chondrogenic cells isolated from chicken limb buds cultured for 2.5 days on 150 µm wide adhesive islands, showing a representative mesenchymal condensation. Cell nuclei are stained blue (DAPI), green indicates positive staining with PNA lectin, and cell-deposited fibronectin is stained red. Scale bar, 100 µm. (*e*) Fluorescent micrographs of pre-chondrogenic cells cultured for 2.5 days on 100 µm wide adhesive islands, showing a representative mesenchymal condensation stained with PNA lectin (green), and for NCAM (red). Scale bar, 50 µm. (Online version in colour.)

placed open at room temperature until dry (figure 1*a*(ii)). The moulds were removed and 3 ml 1% Pluronic F127 (Sigma) in dH_2O was added to each well for 5 min to render the non-coated areas of the well non-adhesive (figure 1*a*(iii)). The wells were washed three times with PBS and stored at 4°C until use. The actual width of the cell adhesive islands was confirmed by measuring the width of 24-h cultures using ImageJ (figure 1*b*,*c*).

2.3. Immunohistochemistry and stainings

After 2.5 days in culture, the samples were fixed in 4% paraformaldehyde in PBS. To identify condensations, the cultures and frozen sections of whole chicken embryos were stained with 50 µg ml^{-1} peanut agglutinin lectin (PNA lectin) conjugated with Alexa Fluor 488 (Invitrogen) in PBS. Cell nuclei were stained with 2 µg ml^{-1} Hoechst 33342 (Invitrogen). To probe for newly synthesized FN, the samples were incubated with a mouse-anti-avian FN antibody (Developmental Studies Hybridoma Bank) and stained with an Alexa Fluor 546 conjugated goat-anti-mouse IgG. Since patterned surfaces in the absence of cells only showed very faint FN staining (data not shown), it can be assumed that the strong FN staining after 2.5 days in culture can be attributed to cell-deposited FN. Expression of neural cell adhesion molecule (NCAM) was probed with a mouse-anti-chicken NCAM antibody (Developmental Studies Hybridoma Bank) and stained with an Alexa Fluor 546 conjugated goat-anti-mouse IgG. A rabbit-anti-Sox9 antibody (Millipore) was used to probe for the expression of Sox9. An Alcian Blue staining was performed to stain for deposited glycosaminoglycans (GAGs). The samples were washed in dH_2O and subsequently stained in 1% Alcian Blue in 3% acetic acid (Electron Microscopy Sciences) for 30 min.

2.4. Quantitative analysis of condensations

To quantify the condensation patterns, micrographs of PNA lectin staining were analysed using ImageJ (v. 1.46r, NIH) and MATLAB (v. R2011a, MathWorks). First, condensations were identified as high intensity regions in the PNA staining-micrographs by applying a threshold to the images (figure 2*b*). Secondly, a size limit was applied in order to exclude small high intensity spots caused by staining artefacts. The coordinates of the centre of mass of the identified condensations were then used to calculate the distance between neighbouring condensations (inter-condensation distance), the number of condensations per unit length and the number of condensations per unit area. Neighbouring condensations were determined as nearest neighbours in the *x*-direction (along the long axis of the island). The 'distance from centre line'-parameter was measured as the shortest distance from the centre of mass of each condensation to an imaginary line drawn through the centre of the adhesive island along its long axis. For the non-patterned substrates, 300 µm wide strips were imaged and analysed in the same manner as the adhesive islands. All parameters were measured per island and then averaged over a range of replicate islands indicated in the figure legends.

2.5. Proliferation assay

To assess proliferation, a ClickiT EdU Alexa Fluor 555 kit (Invitrogen) was used. Samples were incubated with 5 µM EdU for 4 h. For imaging, the samples were fixed with 4% paraformaldehyde, permeabilized with 0.5% Triton X-100 and stained following the manufacturer's protocol for 30 min at room temperature. Nuclei were counterstained with 2 µg ml^{-1} Hoechst 33342. The percentage of proliferating cells was quantified by flow cytometry. After incubation with EdU, the cells were trypsinized to create a single-cell suspension, fixed in 4% paraformaldehyde in PBS and stained following the manufacturer's protocol for 30 min at room temperature. Flow analysis was performed on a BD LSR II Analyzer.

2.6. Glycosaminoglycan quantification

To quantify the deposition of GAGs, a colourimetric dimethyl methylene blue (DMB) assay was used. GAG deposition was normalized to DNA content to obtain GAG/DNA ratios. After 2.5 days in culture, the samples were digested in papain

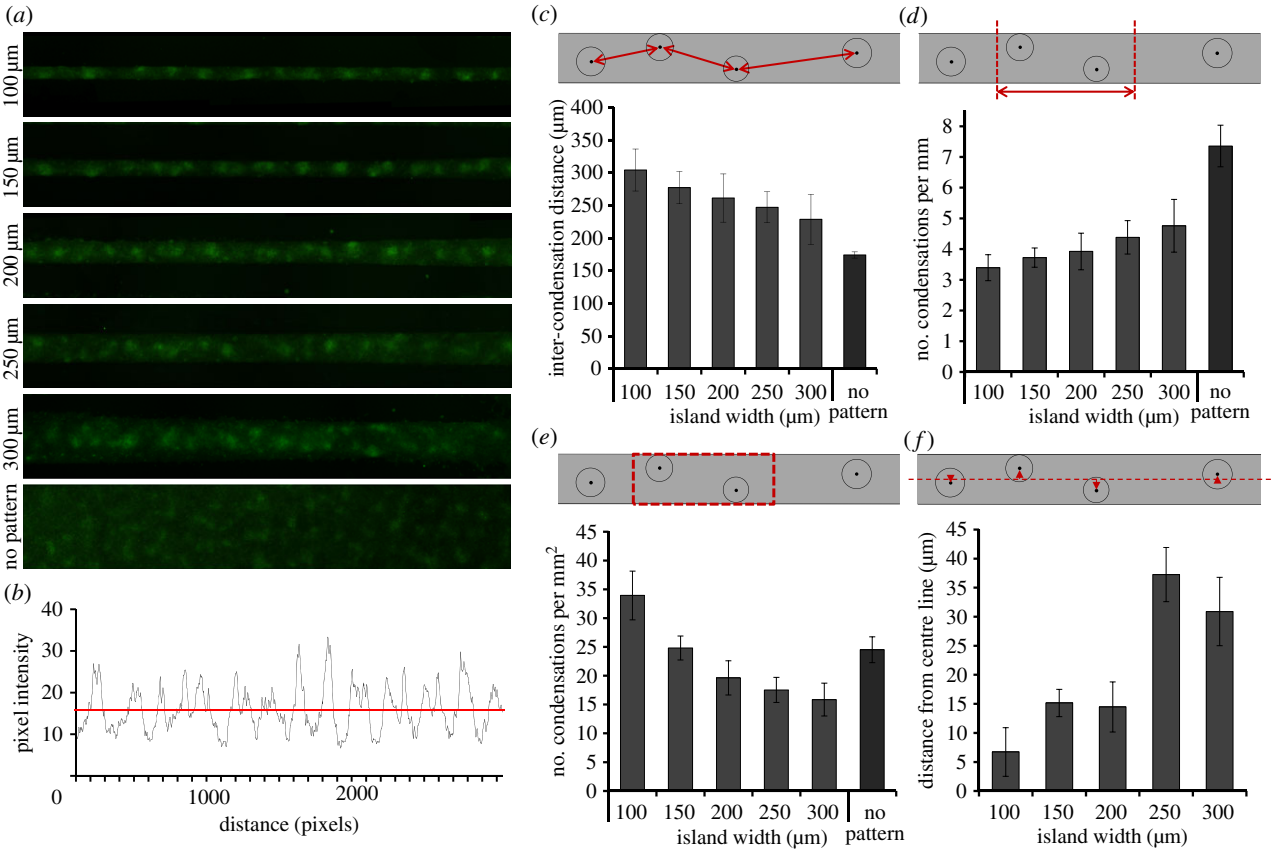

Figure 2. Patterning of condensations under geometric constraints. (*a*) Fluorescent micrographs of PNA lectin staining (green) indicating mesenchymal condensations on linear islands of varying width and on non-patterned substrates after 2.5 days in culture, as used for quantitative analysis. (*b*) Representative intensity plot of PNA lectin staining of cells cultured on a 150 µm wide island for 2.5 days, indicating the pixel intensity along a line drawn along the long axis of the island. The horizontal red line indicates the threshold used for quantitative image analysis to identify the location of the condensations. (*c*) The inter-condensation distance, the distance between neighbouring condensations, is plotted against the width of the adhesive islands. Linear regression analysis shows a statistically significant trend between the inter-condensation distance and the island width (($F = 34.74$) $>$ ($F_{critical} = 7$), $p < 0.0125$). Data represent mean $\pm$ s.d. from $n \geq 7$ 8-mm long islands from two independent experiments. (*d*) Plot of the number of condensations per unit length of adhesive island as a function of the island width. Linear regression analysis shows a statistically significant trend between the number of condensations per unit length and the island width (($F = 27.22$) $>$ ($F_{critical} = 7.09$), $p < 0.0125$). Data represent mean $\pm$ s.d. from $n \geq 6$ 8-mm long islands from two independent experiments. (*e*) The number of condensations per unit area of adhesive island, obtained by dividing the number of condensations per unit length by the island width, is plotted against island width. Linear regression analysis shows a statistically significant trend between the number of condensations per unit area and the island width (($F = 103.47$) $>$ ($F_{critical} = 7.09$), $p < 0.0125$). Data represent mean $\pm$ s.d. from $n \geq 6$ 8-mm long islands from two independent experiments. (*f*) The distance to the centre line is the average distance of the centre of mass of the condensations to a line drawn through the middle of the adhesive island along its long axis. The distance to the centre line is plotted against the island width. Linear regression analysis shows a statistically significant trend between the distance to the centre line and the island width (($F = 63.77$) $>$ ($F_{critical} = 7.4$), $p < 0.0125$). Data represent mean $\pm$ s.d. from $n \geq 5$ 8-mm long islands from two independent experiments. (Online version in colour.)

digestion buffer containing 10 mM L-cysteine and 0.125 mg ml^{-1} papain in PBE buffer (100 mM sodium phosphate buffer, 10 mM Na_2EDTA, pH 6.5) and incubated for 24 h at 65°C. Directly after digestion, the DNA content of the samples was determined using a PicoGreen dsDNA assay kit (Invitrogen) using calf thymus DNA as a standard. A 200× 1,9-dimethyl methylene blue stock solution (3.2 mg ml^{-1}) in 100% ethanol was made to enhance solubility. GAG content was determined by mixing 10 µl sample with 250 µl DMB staining solution (2.37 mg ml^{-1} NaCl, 3.04 mg ml^{-1} glycine, 16 µg ml^{-1} 1,9-dimethyl methylene blue, pH 3) and reading the absorbance at 590 and 525 nm using a BioTek Synergy HT plate reader.

2.7. Sox9 expression

Expression of Sox9 was analysed by flow cytometry. After fixation and permeabilization, cells were probed with a rabbit-anti-Sox9 polyclonal antibody (Millipore) at 5 µg ml^{-1}. Cells were subsequently stained with an Alexa Fluor 647 conjugated goat-anti-rabbit IgG (Invitrogen). Flow analysis was performed on a BD LSR II Analyzer. Mean fluorescent intensities of cell populations retrieved at different time points, as well as freshly isolated cells ('day 0') were used as a measure of Sox9 expression.

2.8. Whole embryo sectioning and analysis

Chicken embryos at Hamburger Hamilton stage 22 were euthanized, washed in PBS and fixed in 4% paraformaldehyde in PBS at 4°C overnight. After multiple PBS washes, the embryos were incubated in 30% sucrose in PBS at 4°C overnight and then in a 50–50 mixture of 30% sucrose in PBS and OCT (Optimal Cutting Temperature, Tissue Tek) at 4°C overnight. Embryos were subsequently embedded in OCT and frozen on dry ice. A Leica cryotome was used to cut 10 µm frozen sections in either the sagittal or the transverse plane of the embryo. Sections were stained with PNA lectin and Hoechst 33342 as described above, and imaged using a Nikon E800 upright microscope. Image analysis was performed using ImageJ to measure the geometric constraint provided to the mesenchymal cells in transverse sections, as well as the inter-condensation distance in sagittal sections.

2.9. Statistics

Linear regression analysis and ANOVA tests were performed using STATA v. 13.0. Linear regression analysis was performed on data for the inter-condensation distance, the number of condensations per unit length, number of condensations per unit area, distance from centre line, Sox9 mean fluorescent intensity, Sox9 pixel intensity and GAG deposition, to test whether a statistical trend was observed between these variables and the island width, by testing whether the slope of the predicted curve was statistically different from zero. The F statistic from each regression analysis was compared with the critical *F*-value at a significance level of $\alpha = 0.05$. Since the inter-condensation distance, the number of condensation per unit length, the number of condensation per unit area and the distance from centreline are derived from the same set of images, a multiple comparison correction is required. For these datasets, the critical *F*-value was therefore determined at a significance level of $\alpha = 0.05/4 = 0.0125$ (Bonferroni correction). One-way ANOVA tests were performed on the data for initial cell density and proliferation on the different island widths to test for significant differences between any of the groups using a significance level of $\alpha = 0.05$. One-tailed unpaired Student's *t*-tests were performed to test whether the Sox9 mean fluorescent intensity, Sox9 pixel intensity and the GAG deposition on 100 μm adhesive islands was significantly different from that on non-patterned substrates.

3. Results

3.1. Experimental model system

In order to study the role of geometric boundary conditions in the formation and patterning of mesenchymal condensations, a microchannel patterning technique was employed to create adhesive islands of specific dimensions (figure 1*a*). The adhesive islands were designed to be 8 mm long and 100, 150, 200, 250 or 300 μm wide, while a continuous FN-coated substrate was used as a negative control (figure 1*b*). The microchannel technique resulted in robust and reproducible patterns, as it was confirmed that the actual island widths closely resembled the desired dimensions (figure 1*c*). Pre-chondrogenic cells were freshly isolated from chicken embryonic limb buds, as it has been demonstrated that these cells are able to form mesenchymal condensations *in vitro* in micromass culture [37]. We adapted the classical micromass culture to conform to our patterned substrates and it was confirmed that typical condensation took place on the adhesive islands (figure 1*d*,*e*). A typical mesenchymal condensation is indicated by a local increase in cell density, positive staining with PNA lectin [15], the deposition of abundant FN matrix and increased expression of the adhesion molecule NCAM [32].

3.2. Patterning of condensations

To investigate the effect of geometric constraints on patterning of condensations, pre-chondrogenic cells were cultured on linear adhesive islands of varying width or on non-patterned substrates. PNA lectin staining revealed mesenchymal condensations (figure 2*a*) and the pixel intensity landscapes were used to identify the locations of individual condensations (figure 2*b*). The distance between the centre of mass of neighbouring condensations, the inter-condensation distance, was measured and compared between the different island sizes. A significant trend was observed, where the inter-condensation distance decreased with increasing island width (figure 2*c*). The inter-condensation distance on non-patterned substrates was smaller than for any of the linear islands. As the inter-condensation distance becomes shorter and the condensations have more room to disperse across the width of the island, as the islands become wider, the number of condensations per millimetre length of adhesive island increased significantly with increasing island width (figure 2*d*). As wider islands contain more cells per millimetre length, the number of condensations per unit area was also determined. Interestingly, a significant downward trend was observed between the number of condensations per unit area and the island width (figure 2*e*). The number of condensations per unit area on the non-patterned substrates was higher than the trend would predict, possibly because cells can be drawn in from outside the quantified region, as it is a continuous culture, resulting in a higher number of condensations. Additionally, the alignment of condensations was evaluated by measuring the distance of the centre of mass of each condensation from the centre line of the island; a line through the middle of the island along its long axis (figure 2*f*). The average distance from the centre line increased significantly with increasing island width; the condensations on the thinnest island (100 μm) had the highest degree of alignment.

3.3. Cell density and proliferation

As the process of condensation is highly dependent on cell density, the initial cell densities on the differently sized islands was quantified to determine whether the observed differences in patterning were simply caused by unequal cell attachment. Initial cell densities on the patterned and non-patterned substrates were found to be not significantly different (figure 3*a*). Furthermore, we investigated the potential effect of the geometric constraints on the proliferation rate as this could result in differences in cell density over time between the differently sized islands, or inhomogeneous cell densities within the islands. Proliferation was assessed after 48 h of culture, while the cells were in the process of condensation. There was no statistically significant difference in proliferation rate between any of the various island sizes (figure 3*b*). Additionally, no regional differences in proliferation were observed on any of the island geometries (figure 3*c*). Apoptosis is assumed not to play a considerable role, as previous studies have shown that apoptosis rates at early time points of *in vitro* condensation are negligible [49].

3.4. Chondrogenic differentiation

Mesenchymal condensation is believed to be the initial step in skeletal development, followed by chondrogenic commitment of the involved cells. We thus investigated whether the geometric constraints imposed on the pre-chondrogenic cells affected their chondrogenic differentiation. Firstly, the expression of the transcription factor Sox9 was investigated, as it is known to play a major role in chondrogenesis during embryonic development and is often used as an early indicator of chondrogenic commitment [50]. Expression of Sox9 at 2.5 days of culture, under all conditions, was increased compared with day 0 (figure 4*a*,*b*). Additionally, at 2.5 days a significant difference was observed between the non-patterned control substrates and the 100 μm islands. When expression levels were compared between the different island sizes, it was found that Sox9 expression decreased when the cells were cultured on wider islands, showing a statistically significant

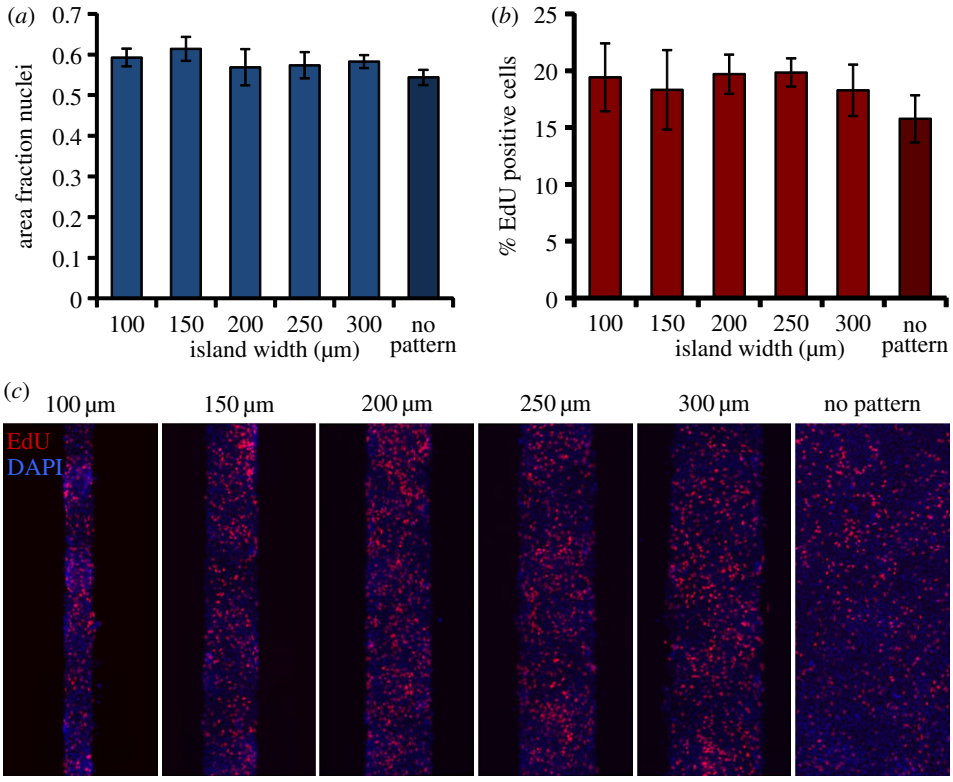

Figure 3. Cell density and proliferation. (*a*) The area fraction occupied by cell nuclei after 1 h in culture, as a measure of initial cell density, is plotted against the island width. None of the differences between conditions is statistically significant. Data represent mean ± s.d., $n = 3$. (*b*) The percentage of proliferating cells at 48 h of culture on adhesive islands, as identified by incorporation of EdU during 4 h of culture, is plotted against the island width. None of the differences between conditions is statistically significant. Data represent mean ± s.d., $n = 4$. (*c*) Fluorescent micrographs of cells cultured on adhesive islands for 48 h, stained for incorporation of EdU (red) and cell nuclei (blue) after 4 h of incubation with EdU. (Online version in colour.)

downward trend. Immunohistochemistry revealed that at 2.5 days Sox9 was located in the nucleus of the cells (figure 4*b*), as expected. The average intensity of the staining of the entire island, as a measure of Sox9 expression, decreased with increasing island width (figure 4*b*,*c*), consistent with the trend observed by flow cytometry (figure 4*a*). While the intensity within the condensations was higher than the average of the entire island on thinner islands, this difference diminished with increasing island width (figure 4*c*). In addition to the early transcription factor Sox9, the deposition of GAGs was quantified. Similar to Sox9 expression, GAG deposition decreased significantly with increasing island width and also the difference between the 100 µm island and the non-patterned substrates was statistically significant (figure 4*d*,*e*).

3.5. Time course of proliferation, condensation and differentiation

In order to gain a better understanding of the temporal sequence of the processes of proliferation, condensation and differentiation on the adhesive islands, these processes were investigated at different time points during the 2.5-day culture. First, it was found that the rate of proliferation was high initially and decreased over time (figure 5*a*). At 24 h, areas of increased cell density started to appear, however typical condensations—indicated by PNA staining—were still absent (figure 5*b*). At 48 h, condensations were visible and they subsequently became more defined over time. In line with the decreasing rate of proliferation and the appearance of condensations, differentiation—indicated by the relative expression of Sox9—increased over time (figure 5*c*).

3.6. Impact of added morphogens

In vivo, tissue development takes place in the presence of various morphogens. To test the effect of specific morphogens on the process of condensation under geometric constraints, cultures were supplemented with varying concentrations and combinations of TGF-β3, BMP2 and FGF8, factors that are known to be involved in the development of the vertebral column [51–54]. In control cultures, after 2.5 days of culture, condensations can be readily identified by increased cell density and positive PNA staining (electronic supplementary material, figure S1). In the presence of a range of concentrations of TGF-β3 or BMP2 however, both the overall cell density and the extent of condensation were reduced. In the presence of FGF8, distinct local increases in cell density are discernable, however PNA staining is more faint. The combination of TGF-β3 and BMP2 resulted in a culture similar to the control condition, while TGF-β3 and FGF8 together lead to distinctive areas of highly increased cell density and considerable PNA staining.

3.7. Patterning of condensations in the chicken embryo

Finally, in order to relate the observed patterning of condensations in our *in vitro* model to patterning *in vivo*, the linear array of condensations of the developing vertebral column was investigated in chicken embryos (figure 6). At Hamburger Hamilton stage 22, the sclerotomal cells that will eventually give rise to the vertebral column have formed a linear pattern of condensations along the body axis, as indicated by PNA lectin staining (figure 6*a*). The neighbouring tissues that provide geometric constraints to this population of cells are the neural tube on the dorsal side, the epithelial

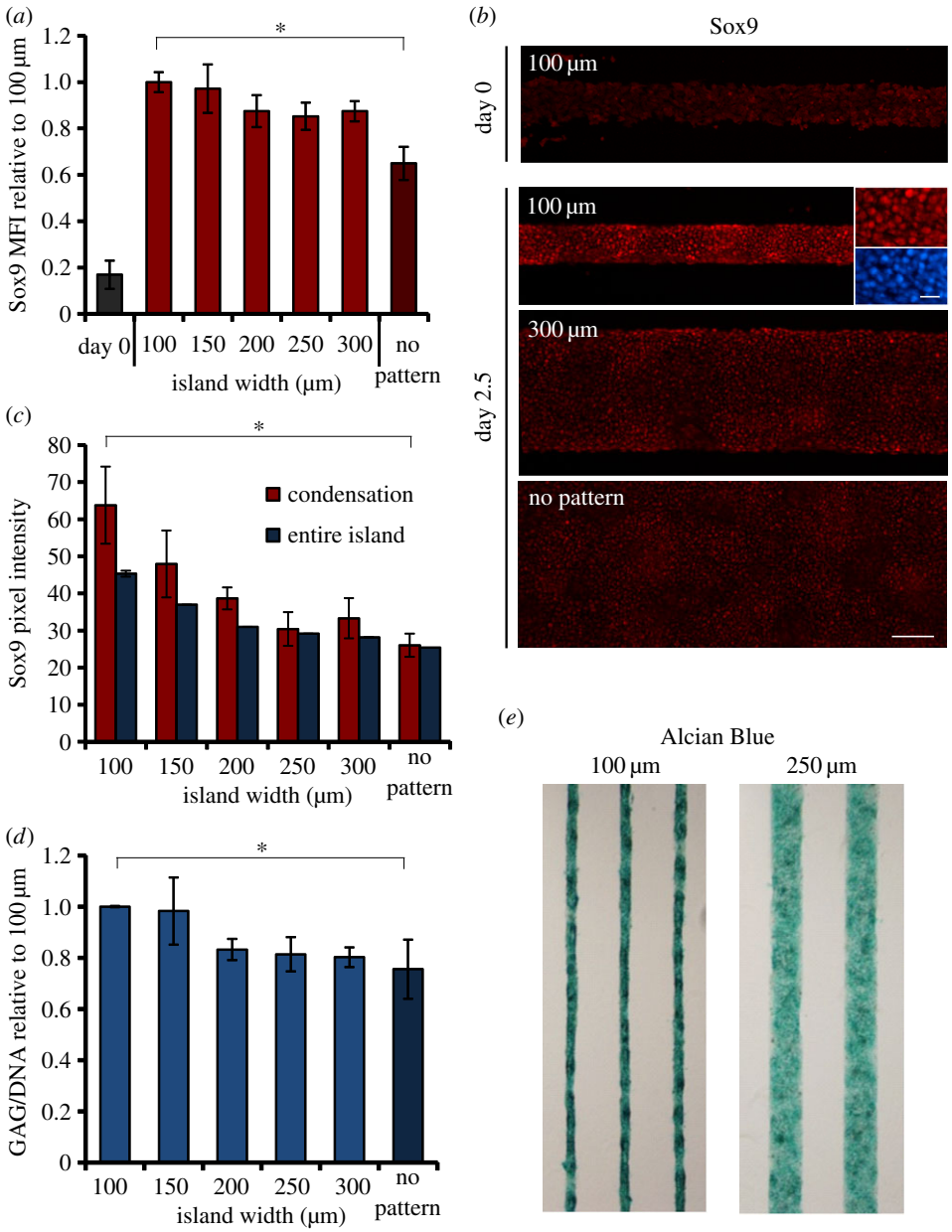

Figure 4. Chondrogenic differentiation under geometric constraints. (*a*) The mean fluorescent intensity of Sox9-stained cells was measured by flow analysis at day 0 (directly after isolation; grey column) and after 2.5 days in culture on adhesive islands of a range of widths and on non-patterned substrates. Data are normalized to the '100 µm' condition. Linear regression analysis shows a statistically significant trend of Sox9 expression at 2.5 days with the island width ($(F = 11.67) > (F_{critical} = 4.41)$, $p < 0.05$). Data represent mean ± s.d., $n = 4$, $^*p < 0.0005$. (*b*) Fluorescent micrographs of immunohistochemistry of Sox9 (red) at day 0 (100 µm, top) and day 2.5 (100, 300 µm and no pattern). A higher magnification of Sox9 (red) and DAPI (nuclei, blue) of the 100 µm island shows the nuclear localization of Sox9 at day 2.5. For the lower magnification, scale bar is 100 µm. For the higher magnification, scale bar is 20 µm. (*c*) The intensity of Sox9 staining was quantified on the entire island and in the condensations and plotted against the islands width. Linear regression analysis shows a statistically significant trend of Sox9 immonufluorescent intensity on the entire island, with the island width ($(F = 35.03) > (F_{critical} = 7.71)$, $p < 0.05$). Data represent mean ± s.d., $n = 10$, $^*p < 0.0005$. (*d*) GAG content was quantified for 2.5-day cultures and normalized to DNA content. The data are presented relative to the '100 µm' condition. Linear regression analysis shows a statistically significant trend of GAG/DNA content with the island width ($(F = 16.74) > (F_{critical} = 4.75)$, $p < 0.05$). Data represent mean ± s.d., $n = 3$, $^*p < 0.05$. (*e*) Colour micrographs of 2.5-day cultures stained with Alcian Blue, indicating the deposition of GAGs on 100 versus 250 µm islands. (Online version in colour.)

dermamyotome on the dorsal–lateral sides and the notochord and aorta medially (figure 6*a*). At this stage, the width of the sclerotomal cell population constrained within the transverse plane was measured to be 171 ± 19 µm. The inter-condensation distance was measured in the sagittal plane and had a mean value of 251 ± 20 µm (figure 6*b*).

4. Discussion

The role of physical cues in the creation of the characteristic pattern of the vertebral column has not been widely explored. This study addresses the hypothesis that geometric constraints play a role in determining the linear pattern of condensations at the onset of the development of the vertebral column. By employing a novel *in vitro* model, we found that the spacing and alignment of condensations, as well as the number of condensation per unit area, were influenced by the geometry of the cell adhesive pattern. Interestingly, measurements of the spatial constraints of the developing vertebral column in the chicken embryo and its pattern of condensations were shown to closely fit into the quantitative relation between geometric constraints and inter-condensation distance found *in vitro*.

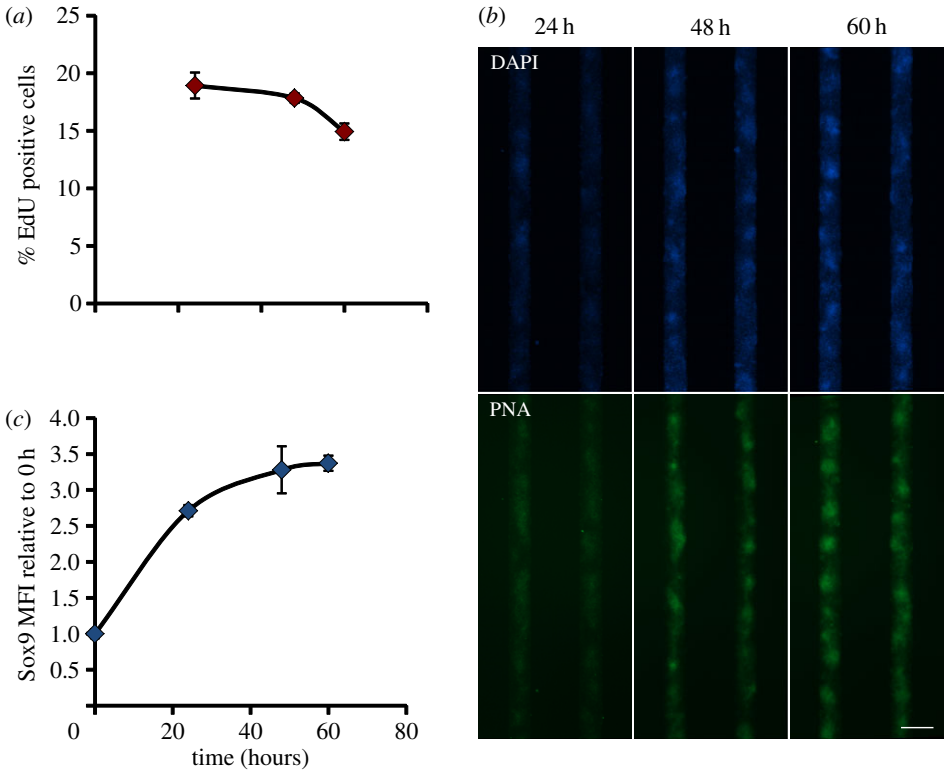

Figure 5. Time course of proliferation, condensation and differentiation. (*a*) The percentage of proliferating cells on 150 μm wide adhesive islands, as identified by incorporation of EdU during 4 h of culture, is plotted against time. Data represent mean ± s.d., $n = 3$. (*b*) Fluorescent micrographs of pre-chondrogenic cells cultured on 150 μm wide adhesive islands stained with DAPI (blue, cell nuclei), and PNA lectin (green, indicating condensations) at 24, 48 and 60 h. Scale bar is 200 μm. (*c*) The Sox9 mean fluorescent intensity of cells retrieved from 150 μm wide adhesive islands, as measured by flow cytometry, is plotted against time. Data represent mean ± s.d., $n = 3$. (Online version in colour.)

The distance between neighbouring condensations, the inter-condensation distance, was shown to increase significantly when skeletal precursor cells were cultured on linear adhesive islands of decreasing width (figure 2*c*). Condensation is defined by an increase in local cell density [16,19]. A minimum number of cells must be drawn together to create a condensation [55] and the process is thus dependent on cell availability. On the thinner islands, fewer cells are available along the short axis, so this could explain why the inter-condensation distance increases and the number of condensations per unit island length decreases with decreasing island width. If the spacing of condensations was only a function of cell availability, the number of condensations per unit area would presumably be constant. We found a different trend, however, implying that the mechanism that governs the patterning of condensations is more complex. The process of condensation involves a fine balance between the cohesiveness of cells versus their interaction with the extracellular matrix. As varying geometric constraints will alter the ratio between perimeter and surface area, this might shift the balance between cell–cell versus cell–matrix contacts and the cellular forces applied at those contacts, as indicated by several investigations on force generation by multicellular cultures [46,47,56]. Theoretical models have indicated these forces as key players in the condensation process [24,57,58]. Further investigations are needed to unravel the mechanisms that cause the difference in patterning of condensations under varying geometric constraints.

Interestingly, the *in vivo* inter-condensation distance and geometric constraints of the developing vertebral column, measured in chicken embryos, were found to closely fit into the quantitative relation described by the *in vitro* model (figure 6). The *in vitro* model is limited in its capacity to capture all aspects of the *in vivo* condensation process, as it does not recapitulate the full three-dimensional environment or possible signalling events from nearby epithelium implied to be involved in the process of condensation [59]. Remarkably, despite these discrepancies, the isolated mesenchymal cells are able to form condensations on the provided adhesive islands in specific patterns that match the condensation pattern in the developing vertebral column *in vivo*. This can thus be seen as a process of self-organization, as *in vitro* this is not orchestrated by signalling from neighbouring tissues.

In the developing vertebral column, the condensations are not only consistently spaced, but they are also accurately aligned along the body axis, which is critical for the eventual structure of the spine. The distance of the centre of mass of each condensation to the centre line of the island was quantified in this study (figure 2*f*) as a measure of alignment. A significant trend was found, with the distance diminishing for the thinnest islands. The enhanced alignment of condensations on thinner islands reflects the more limited space for the condensations to disperse. Similarly, if the population of cells in the *in vivo* environment of the developing spine is spatially restricted, the condensations may also be forced to align.

Geometric boundary conditions have been previously shown to play a role in a variety of cellular events. In the context of the developing embryo, it was shown that elongation of the body axis in *Xenopus* embryos is a process of self-organization controlled by physical alignment cues from the edges of the cell population [60]. Additionally, anterior–posterior axis polarization in mouse embryos is indicated to be triggered by

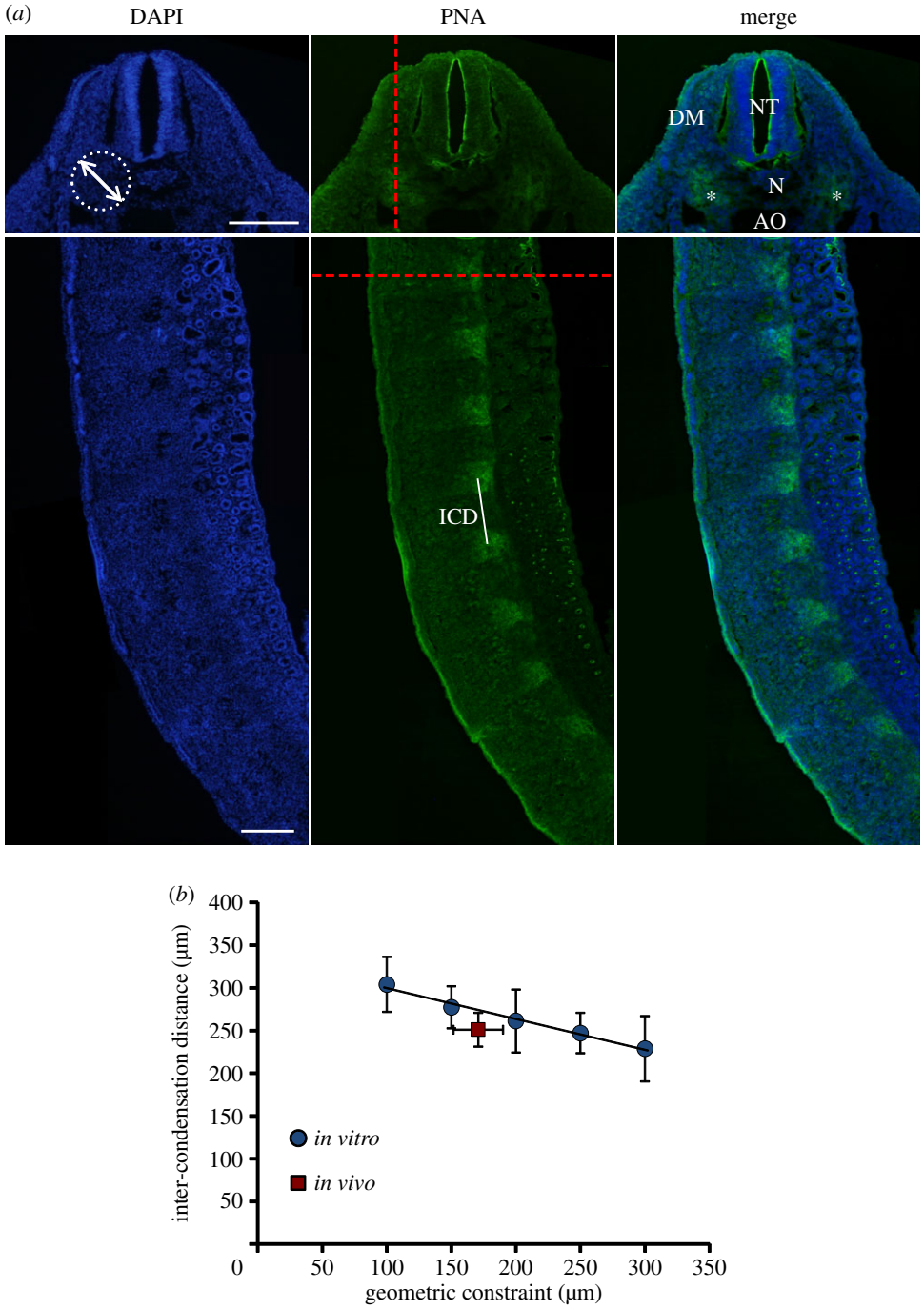

Figure 6. Patterning of condensations *in vivo*. (*a*) Fluorescent micrographs of transverse (top) and sagittal (bottom) sections of a chicken embryo at HH stage 22. Cell nuclei are stained blue (left) and PNA lectin staining is indicated in green (middle). Red dashed line in transverse section indicates the cross-sectional plane of the sagittal section and vice-versa. The white dashed circle indicates the estimated geometric constraint of the population of sclerotomal cells. Neighbouring tissues that provide the spatial constraints are the neural tube (NT), the dermamyotome (DM), the notochord (N) and the aorta (AO). Mesenchymal condensations in the transverse plane are indicated with an asterisk (*). The inter-condensation distance (ICD) is indicated in the sagittal section. Scale bars, 200 μm. (*b*) The inter-condensation distance is plotted against the geometric constraint for the *in vitro* model (also in figure 2*c*) as well as the chicken embryo (*in vivo*). For the *in vitro* model, the geometric constraint on the *x*-axis indicates the island width, while for the *in vivo* case it indicates the measured width of the population of sclerotomal cells (indicated by the white dashed circle in (*a*)). Data represent mean ± s.d. from 20 measurements from three embryos. (Online version in colour.)

the boundary conditions that the uterine wall provides to the early embryo [61]. In this study, we show the effect of geometric constraints on the supracellular process of patterning of mesenchymal condensations.

Morphogens are soluble factors that are thought to play an important role in pattern formation and tissue development *in vivo*. The effect of three relevant morphogens—TGF-β3, BMP2 and FGF8—on the condensation process was tested on 171 μm adhesive islands, based on the measured tissue width *in vivo* (figure 6). The addition of TGF-β3 or BMP2 had an inhibiting effect on proliferation and condensation, as indicated by the decreased cell density and faint PNA staining when compared with control cultures (electronic supplementary material, figure S1). FGF8, either alone or in combination with the other morphogens, caused a strong increase in local cell densities, however the faint PNA staining in the majority of these conditions indicates that these areas of increased cell density might not represent characteristic condensations. Possibly, FGF8 reduces cell–matrix adhesion, causing the cells to cluster in a non-specific

manner. In contrast to the static presence of morphogens in this study, during tissue development *in vivo* morphogens are secreted at specific locations at specific times, resulting in complex spatial and temporal gradients [53,62]. More complex model systems are required to further elucidate the interplay between geometric constraints and morphogen gradients in patterning and differentiation.

To test whether chondrogenic lineage commitment was affected by the imposed geometric constraints in our model system, the expression of Sox9 and extent of GAG deposition were also investigated (figure 4). Both Sox9 expression and GAG deposition decreased significantly as the islands became wider, indicating that the overall chondrogenic differentiation was enhanced on substrates with tighter geometric constraints. For both differentiation markers, a significant difference was observed between the non-patterned control substrates and the 100 µm islands. These findings correspond with the observation that the number of condensations per unit area is increased on thinner islands. Moreover, on the thinner islands the difference in intensity of Sox9 expression between condensations and the rest of the island was more pronounced than on wider islands. This might indicate that the condensations are more mature, in terms of chondrogenic differentiation, under tighter geometric constraints. It has been shown previously that the extent of chondrogenic differentiation from condensations can be modulated by various soluble factors [63,64], but the observed effect of geometric constraints provides new insight into the role of physical cues in the differentiation process.

Taken together, this study suggests a role for geometric boundary conditions in regulating skeletal patterning during embryonic development in a process of self-organization. The pattern of condensations in the chicken embryo was shown to closely fit the relationship found *in vitro*. Different species with varying dimensions could be studied in the future to investigate whether this relationship extends to other vertebrates as well. Moreover, further experimentation could provide more insight into the mechanisms involved and the possible impact of geometric constraints on additional developmental processes. This line of investigations is likely to provide a more profound understanding of the processes of tissue patterning and morphogenesis.

Acknowledgements. The authors would like to thank Alan Rodrigues and Clifford Tabin for sharing their expertise on chicken embryo limb bud cell isolations, Cristiana Cunha for help with flow cytometry experiments and Max Darnell for help with statistical analysis.

Funding statement. This work was funded by National Institute of Health (R37 DE013033), ZonMW-VICI grant no. 918.11.635 (The Netherlands), and Research Institute MOVE at the VU University, Amsterdam. A.S.M. acknowledges funding from the National Science Foundation Graduate Research Fellowships Program, and T.H.S. was supported by a visiting scholarship from the Wyss Institute for Biologically Inspired Engineering at Harvard University.

References

1. Gjorevski N, Nelson CM. 2010 The mechanics of development: models and methods for tissue morphogenesis. *Birth Defects Res. C Embryo Today* **90**, 193–202. (doi:10.1002/bdrc.20185)
2. Ingber DE. 2006 Mechanical control of tissue morphogenesis during embryological development. *Int. J. Dev. Biol.* **50**, 255–266. (doi:10.1387/ijdb.052044di)
3. Mammoto T, Ingber DE. 2010 Mechanical control of tissue and organ development. *Development* **137**, 1407–1420. (doi:10.1242/dev.024166)
4. Nowlan NC, Murphy P, Prendergast PJ. 2007 Mechanobiology of embryonic limb development. *Ann. N Y Acad. Sci.* **1101**, 389–411. (doi:10.1196/annals.1389.003)
5. Wozniak MA, Chen CS. 2009 Mechanotransduction in development: a growing role for contractility. *Nat. Rev. Mol. Cell Biol.* **10**, 34–43. (doi:10.1038/nrm2592)
6. Savin T, Kurpios NA, Shyer AE, Florescu P, Liang H, Mahadevan L, Tabin CJ. 2011 On the growth and form of the gut. *Nature* **476**, 57–62. (doi:10.1038/nature10277)
7. Shyer AE, Tallinen T, Nerurkar NL, Wei Z, Gil ES, Kaplan DL, Tabin CJ, Mahadevan L. 2013 Villification: how the gut gets its villi. *Science* **342**, 212–218. (doi:10.1126/science.1238842)
8. Beloussov LV, Grabovsky VI. 2006 Morphomechanics: goals, basic experiments and models. *Int. J. Dev. Biol.* **50**, 81–92. (doi:10.1387/ijdb.052056lb)
9. Brodland GW *et al*. 2010 Video force microscopy reveals the mechanics of ventral furrow invagination in *Drosophila*. *Proc. Natl Acad. Sci. USA* **107**, 22 111–22 116. (doi:10.1073/pnas.1006591107)
10. Gjorevski N, Nelson CM. 2010 Endogenous patterns of mechanical stress are required for branching morphogenesis. *Integr. Biol.* (*Camb*) **2**, 424–434. (doi:10.1039/c0ib00040j)
11. Christ B, Huang R, Wilting J. 2000 The development of the avian vertebral column. *Anat. Embryol.* (*Berl*) **202**, 179–194. (doi:10.1007/s004290000114)
12. Smith LJ, Nerurkar NL, Choi KS, Harfe BD, Elliott DM. 2011 Degeneration and regeneration of the intervertebral disc: lessons from development. *Dis. Model Mech.* **4**, 31–41. (doi:10.1242/dmm.006403)
13. DeLise AM, Fischer L, Tuan RS. 2000 Cellular interactions and signaling in cartilage development. *Osteoarthritis Cartilage* **8**, 309–334. (doi:10.1053/joca.1999.0306)
14. Hall BK. 1987 Earliest evidence of cartilage and bone development in embryonic life. *Clin. Orthop. Relat. Res.* **255**, 255–272.
15. Hall BK, Miyake T. 1992 The membranous skeleton: the role of cell condensations in vertebrate skeletogenesis. *Anat. Embryol.* (*Berl*) **186**, 107–124. (doi:10.1007/BF00174948)
16. Thorogood PV, Hinchliffe JR. 1975 An analysis of the condensation process during chondrogenesis in the embryonic chick hind limb. *J. Embryol. Exp. Morphol.* **33**, 581–606.
17. Grüneberg H. 1963 *The pathology of development: a study of inhereted skeletal disorders in animals*. Oxford, UK: Blackwells Scientific Publications.
18. Hall BK, Miyake T. 2000 All for one and one for all: condensations and the initiation of skeletal development. *Bioessays* **22**, 138–147. (doi:10.1002/(SICI)1521-1878(200002)22:2<138::AID-BIES5>3.0.CO;2-4)
19. Hall BK, Miyake T. 1995 Divide, accumulate, differentiate: cell condensation in skeletal development revisited. *Int. J. Dev. Biol.* **39**, 881–893.
20. Janners MY, Searls RL. 1970 Changes in rate of cellular proliferation during the differentiation of cartilage and muscle in the mesenchyme of the embryonic chick wing. *Dev. Biol.* **23**, 136–165. (doi:10.1016/S0012-1606(70)80011-2)
21. Summerbell D, Wolpert L. 1972 Cell density and cell division in the early morphogenesis of the chick wing. *Nat. New Biol.* **239**, 24–26. (doi:10.1038/newbio239024a0)
22. Cui C. 2005 *Dynamics of cell movement and tissue motion in gastrulation and micromass cell culture*. Bloomington, IN: Indiana University.
23. Newman SA, Frenz DA, Tomasek JJ, Rabuzzi DD. 1985 Matrix-driven translocation of cells and nonliving particles. *Science* **228**, 885–889. (doi:10.1126/science.4001925)
24. Oster GF, Murray JD, Maini PK. 1985 A model for chondrogenic condensations in the developing limb:

the role of extracellular matrix and cell tractions. *J. Embryol. Exp. Morphol.* **89**, 93–112.

25. Dessau W, von der Mark H, von der Mark K, Fischer S. 1980 Changes in the patterns of collagens and fibronectin during limb-bud chondrogenesis. *J. Embryol. Exp. Morphol.* **57**, 51–60.
26. Knudson CB, Toole BP. 1985 Changes in the pericellular matrix during differentiation of limb bud mesoderm. *Dev. Biol.* **112**, 308–318. (doi:10.1016/0012-1606(85)90401-4)
27. Kulyk WM, Upholt WB, Kosher RA. 1989 Fibronectin gene expression during limb cartilage differentiation. *Development* **106**, 449–455.
28. Stern CD. 1984 Mini-review: hyaluronidases in early embryonic development. *Cell Biol. Int. Rep.* **8**, 703–717. (doi:10.1016/0309-1651(84)90108-5)
29. Tomasek JJ, Mazurkiewicz JE, Newman SA. 1982 Nonuniform distribution of fibronectin during avian limb development. *Dev. Biol.* **90**, 118–126. (doi:10.1016/0012-1606(82)90217-2)
30. Oberlender SA, Tuan RS. 1994 Expression and functional involvement of N-cadherin in embryonic limb chondrogenesis. *Development* **120**, 177–187.
31. Tavella S, Raffo P, Tacchetti C, Cancedda R, Castagnola P. 1994 N-CAM and N-cadherin expression during *in vitro* chondrogenesis. *Exp. Cell Res.* **215**, 354–362. (doi:10.1006/excr.1994.1352)
32. Widelitz RB, Jiang TX, Murray BA, Chuong CM. 1993 Adhesion molecules in skeletogenesis: II. Neural cell adhesion molecules mediate precartilaginous mesenchymal condensations and enhance chondrogenesis. *J. Cell Physiol.* **156**, 399–411. (doi:10.1002/jcp.1041560224)
33. Hui TY, Cheung KM, Cheung WL, Chan D, Chan BP. 2008 *In vitro* chondrogenic differentiation of human mesenchymal stem cells in collagen microspheres: influence of cell seeding density and collagen concentration. *Biomaterials* **29**, 3201–3212. (doi:10.1016/j.biomaterials.2008.04.001)
34. Mauck RL, Seyhan SL, Ateshian GA, Hung CT. 2002 Influence of seeding density and dynamic deformational loading on the developing structure/function relationships of chondrocyte-seeded agarose hydrogels. *Ann. Biomed. Eng.* **30**, 1046–1056. (doi:10.1114/1.1512676)
35. Centola M, Tonnarelli B, Scharen S, Glaser N, Barbero A, Martin I. 2013 Priming 3D cultures of human mesenchymal stromal cells toward cartilage formation via developmental pathways. *Stem Cells Dev.* **22**, 2849–2858. (doi:10.1089/scd.2013.0216)
36. ten Berge D, Brugmann SA, Helms JA, Nusse R. 2008 Wnt and FGF signals interact to coordinate growth with cell fate specification during limb development. *Development* **135**, 3247–3257. (doi:10.1242/dev.023176)
37. Ahrens PB, Solursh M, Reiter RS. 1977 Stage-related capacity for limb chondrogenesis in cell culture. *Dev. Biol.* **60**, 69–82. (doi:10.1016/0012-1606(77)90110-5)
38. DeLise AM, Stringa E, Woodward WA, Mello MA, Tuan RS. 2000 Embryonic limb mesenchyme micromass culture as an *in vitro* model for chondrogenesis and cartilage maturation. *Methods Mol. Biol.* **137**, 359–375. (doi:10.1385/1-59259-066-7:359)
39. Denker AE, Haas AR, Nicoll SB, Tuan RS. 1999 Chondrogenic differentiation of murine C3H10T1/2 multipotential mesenchymal cells: I. Stimulation by bone morphogenetic protein-2 in high-density micromass cultures. *Differentiation* **64**, 67–76. (doi:10.1046/j.1432-0436.1999.6420067.x)
40. Denker AE, Nicoll SB, Tuan RS. 1995 Formation of cartilage-like spheroids by micromass cultures of murine C3H10T1/2 cells upon treatment with transforming growth factor-beta 1. *Differentiation* **59**, 25–34. (doi:10.1046/j.1432-0436.1995.5910025.x)
41. Bhat R, Lerea KM, Peng H, Kaltner H, Gabius HJ, Newman SA. 2011 A regulatory network of two galectins mediates the earliest steps of avian limb skeletal morphogenesis. *BMC Dev. Biol.* **11**, 6. (doi:10.1186/1471-213X-11-6)
42. Woods A, Wang G, Dupuis H, Shao Z, Beier F. 2007 Rac1 signaling stimulates N-cadherin expression, mesenchymal condensation, and chondrogenesis. *J. Biol. Chem.* **282**, 23 500–23 508. (doi:10.1074/jbc.M700680200)
43. Thery M. 2010 Micropatterning as a tool to decipher cell morphogenesis and functions. *J. Cell Sci.* **123**, 4201–4213. (doi:10.1242/jcs.075150)
44. Chen CS, Mrksich M, Huang S, Whitesides GM, Ingber DE. 1997 Geometric control of cell life and death. *Science* **276**, 1425–1428. (doi:10.1126/science.276.5317.1425)
45. Li B, Li F, Puskar KM, Wang JH. 2009 Spatial patterning of cell proliferation and differentiation depends on mechanical stress magnitude. *J. Biomech.* **42**, 1622–1627. (doi:10.1016/j.jbiomech.2009.04.033)
46. Nelson CM, Jean RP, Tan JL, Liu WF, Sniadecki NJ, Spector AA, Chen CS. 2005 Emergent patterns of growth controlled by multicellular form and mechanics. *Proc. Natl Acad. Sci. USA* **102**, 11 594–11 599. (doi:10.1073/pnas.0502575102)
47. Ruiz SA, Chen CS. 2008 Emergence of patterned stem cell differentiation within multicellular structures. *Stem Cells* **26**, 2921–2927. (doi:10.1634/stemcells.2008-0432)
48. Hamburger V, Hamilton H. 1951 A series of normal stages in the development of the chick embryo. *J. Morphol.* **88**, 49–92. (doi:10.1002/jmor.1050880104)
49. Coleman CM, Tuan RS. 2003 Growth/differentiation factor 5 enhances chondrocyte maturation. *Dev. Dyn.* **228**, 208–216. (doi:10.1002/dvdy.10369)
50. Bi W, Deng JM, Zhang Z, Behringer RR, de Crombrugghe B. 1999 Sox9 is required for cartilage formation. *Nat. Genet.* **22**, 85–89. (doi:10.1038/8792)
51. Brent AE, Tabin CJ. 2004 FGF acts directly on the somitic tendon progenitors through the Ets transcription factors *Pea3* and *Erm* to regulate scleraxis expression. *Development* **131**, 3885–3896. (doi:10.1242/dev.01275)
52. Huang R, Stolte D, Kurz H, Ehehalt F, Cann GM, Stockdale FE, Patel K, Christ B. 2003 Ventral axial organs regulate expression of myotomal *Fgf-8* that influences rib development. *Dev. Biol.* **255**, 30–47. (doi:10.1016/S0012-1606(02)00051-9)
53. Roberts AB, Sporn MB. 1992 Differential expression of the TGF-beta isoforms in embryogenesis suggests specific roles in developing and adult tissues. *Mol. Reprod. Dev.* **32**, 91–98. (doi:10.1002/mrd.1080320203)
54. Wan M, Cao X. 2005 BMP signaling in skeletal development. *Biochem. Biophys. Res. Commun.* **328**, 651–657. (doi:10.1016/j.bbrc.2004.11.067)
55. Cottrill CP, Archer CW, Wolpert L. 1987 Cell sorting and chondrogenic aggregate formation in micromass culture. *Dev. Biol.* **122**, 503–515. (doi:10.1016/0012-1606(87)90314-9)
56. Kim JH *et al*. 2013 Propulsion and navigation within the advancing monolayer sheet. *Nat. Mater.* **12**, 856–863. (doi:10.1038/nmat3689)
57. Bard JB. 1990 Traction and the formation of mesenchymal condensations *in vivo*. *Bioessays* **12**, 389–395. (doi:10.1002/bies.950120809)
58. Murray JD, Oster GF. 1984 Cell traction models for generating pattern and form in morphogenesis. *J. Math. Biol.* **19**, 265–279. (doi:10.1007/BF00277099)
59. Mammoto T *et al*. 2011 Mechanochemical control of mesenchymal condensation and embryonic tooth organ formation. *Dev. Cell* **21**, 758–769. (doi:10.1016/j.devcel.2011.07.006)
60. Green JB, Dominguez I, Davidson LA. 2004 Self-organization of vertebrate mesoderm based on simple boundary conditions. *Dev. Dyn.* **231**, 576–581. (doi:10.1002/dvdy.20163)
61. Hiramatsu R, Matsuoka T, Kimura-Yoshida C, Han SW, Mochida K, Adachi T, Takayama S, Matsuo I. 2013 External mechanical cues trigger the establishment of the anterior–posterior axis in early mouse embryos. *Dev. Cell* **27**, 131–144. (doi:10.1016/j.devcel.2013.09.026)
62. Tabata T, Takei Y. 2004 Morphogens, their identification and regulation. *Development* **131**, 703–712. (doi:10.1242/dev.01043)
63. Hatakeyama Y, Tuan RS, Shum L. 2004 Distinct functions of BMP4 and GDF5 in the regulation of chondrogenesis. *J. Cell Biochem.* **91**, 1204–1217. (doi:10.1002/jcb.20019)
64. Sohn P, Cox M, Chen D, Serra R. 2010 Molecular profiling of the developing mouse axial skeleton: a role for Tgfbr2 in the development of the intervertebral disc. *BMC Dev. Biol.* **10**, 29. (doi:10.1186/1471-213X-10-29)